

PAPER

CrossMark
click for updatesCite this: *RSC Adv.*, 2016, 6, 67586

Spin phase protection in interference of electron spin waves in lightly hydrogenated graphene†

T. Kato,^a J. Kamijo,^a T. Nakamura,^b C. Ohata,^a S. Katsumoto^b and J. Haruyama^{*a}

Electron spin transport in graphene is extremely sensitive to foreign atoms and ripples of the SiO₂ substrate. Indeed, the observed spin diffusion- and relaxation-length (time) were smaller than theoretically expected owing to this, although a large spin diffusion length has been recently realized in graphene synthesized on a SiC substrate. It is, thus, crucial to enhance the spin phase coherence and spin diffusion (relaxation) length of a graphene/SiO₂ substrate particularly for future graphene spintronics. One of the approaches to realize this is the investigation of the spin phase in the phase interference phenomena of electron spin waves (such as weak localization (WL)) and its correlation with the spin-orbit-interaction (SOI). However, their coexistence in graphene is difficult to be realized experimentally. Here, we have realized the extremely light hydrogenation of a graphene surface ($\ll 0.1\%$) on SiO₂ by precisely controlling the amount of electron beam (EB) irradiation to a specific EB resist including hydrogen atoms, treated on graphene. It allows the coexistence of WL and the SOI. We find spin phase protection (suppression of dephasing) of the electron-spin-waves in the WL on temperature and external magnetic-field dependence in the graphenes with hydrogenation volumes (N_{H}) as small as 0.06%. As an origin, correlation of the WL with a Rashba-type SOI, which can be introduced by out-of-plane symmetry breaking due to the formation of sp³ bonds derived from the small N_{H} , is discussed. The present finding in lightly hydrogenated graphene must be beneficial for graphene spintronics, which requests a long spin diffusion- and coherence-length. It will realize a possible 2D-topological insulating state in graphene.

Received 9th May 2016
Accepted 2nd July 2016

DOI: 10.1039/c6ra11648e

www.rsc.org/advances

Introduction

Spintronics are highly promising as a key technology for the next generation.^{1,2} They provide the following two prospects: (1) zero-emission energy and (2) replacement of CMOS technology (*i.e.*, beyond CMOS). From the first prospect, spin currents carry and emit no energy and no heat. This strong advantage resolves heat problems in large-scale integration circuits, personal computers, and also any systems loading them. In particular, heat problems become much more significant in highly enclosed spaces (*e.g.*, in aerospace and on aeroplanes). Spintronic devices and circuits must be tremendously effective for such systems. From the second prospect, it is a desirable subject to realize devices beyond CMOS FETs, which are approaching their integration and operational limits. Although various materials and technologies have endeavoured to realize this, it has not yet been realized. Spintronic devices based on some kinds of ideas must realize this challenge. For instance, operation utilizing spin flipping leads to extremely high switching

devices (*e.g.*, in picoseconds), which overcomes the operation speeds of CMOS FETs and LSIs. Spin quantum bits also enable the treatment of large amounts of information by a much smaller-scale integration compared to CMOS circuits. Therefore, spintronic devices are desired for future key technologies.

On the other hand, graphene, a carbon mono-atomic layer, has recently emerged following the discovery of an easy fabrication method, the so-called mechanical exfoliation of graphite. Strong spin coherence and large diffusion length have been highly expected in graphene because of the weak spin-orbit interaction (SOI) due to the small mass and weak hyperfine interactions, which are unique to carbon atoms. Some literatures, however, reported on the weak spin-coherence and -diffusion of graphene on a SiO₂ substrate owing to the bad influence of the substrate (*e.g.*, impurities, ripples), while only few works reported on the strong coherence, as predicted by the theories. Because graphene is a mono-atomic layer directly fabricated on substrates, indeed such substrates factor significantly and certainly reduce the spin coherence and diffusion. Avoiding these factors (*e.g.*, by utilizing hexagonal-boron-nitride (h-BN) and SiC substrates) enables the fabrication of highly effective spintronic devices with a strong spin coherence.

Here, when the sample size is smaller than or comparable to the phase coherence length L_{ϕ} or thermal diffusion length L_{th} (*i.e.*, within a diffusive electron transport regime), the phase

^aFaculty of Science and Engineering, Aoyama Gakuin University, 5-10-1 Fuchinobe, Sagami-hara, Kanagawa 252-5258, Japan. E-mail: J-haru@ee.aoyama.ac.jp

^bInstitute for Solid State Physics, The University of Tokyo, 5-1-5 Kashiwanoha, Kashiwa, Chiba 277-8581, Japan

† Electronic supplementary information (ESI) available. See DOI: 10.1039/c6ra11648e

memory of the electron spin waves is preserved over the entire sample region even with electron scattering by disorder.^{1,2} This introduces various famous phase interference phenomena of the electron spin waves in thin metals, semiconductor 2D electron gas (2DEG), and carbon nanotubes (CNTs) (ESI 1†);^{1–8} e.g., WL (which is a constructive phase interference between two partial electron waves within the same phase encircling a 2D plane in opposite directions along time-reversal symmetry paths. It shows a magnetoresistance (MR) peak with negative MR due to dephasing caused by applying an external perpendicular-magnetic field (B_{\perp})).

Observation of the strength of the WL on temperature and B_{\perp} changes allows the confirmation of enhanced spin coherence and relaxation. Indeed, spin relaxation time enhanced by the presence of magnetic defects and subsequently large-magnitude WL were reported in graphene.^{5,6} A large spin diffusion length has been recently reported in a graphene/SiC substrate.^{7,8} Moreover, a significant increase in the spin relaxation length (up to 7 μm) was observed due to Rashba-type SOI for a plasma-hydrogenated graphene with a hydrogen volume $N_{\text{H}} = 0.02\%$.¹² It has also been theoretically reported that in out-of-plane mirror-symmetric SOI systems like graphene, an effective B due to a SOI (B_{SOI}) suppresses dephasing in the WL and does not cause spin-flipping (*i.e.*, anti-localization (AL), which is a destructive interference with a phase difference in π caused from the WL by a spin flip that exhibits a MR minimum).¹⁶ When a Berry phase factor (β/π) is smaller than 0.6 in graphene, B_{SOI} also suppresses the WL because B_{SOI} (*i.e.*, a random Rashba field) acts like a magnetic scattering centre.⁹

Therefore, observation of the WL associated with SOI, introduced by the out-of-plane symmetry breaking due to sp^3 bonds formed by the light hydrogenation, is highly interesting and useful for graphene spintronics. However, the coexistence of the WL with SOIs in graphene is difficult to be experimental realized. A heavy volume of adatoms (*e.g.*, $N_{\text{H}} \gg 0.1\%$) forms a diffusive charge-transport regime inducing WL, while destroying SOIs. In contrast, a small N_{H} (*e.g.*, $\ll 0.05\%$) results in a ballistic charge-transport regime introducing SOIs, while decreasing the WL. Precise control of N_{H} to cause WL is, thus, crucial to produce the crossover region between these two regimes (*e.g.*, $0.05\% < N_{\text{H}} < 0.1\%$) in graphene and reveal the unique behaviours.

Experimental and discussion

Sample preparation and characterization

In the present experiment, a hydrogen silsesquioxane (HSQ) resist [(HSiO_{3/2})_{*n*}] has been treated on pristine graphene mechanically exfoliated from HOPG and placed on SiO₂.^{10,11} When the HSQ resist is irradiated with an electron beam (EB), H atoms detach from the resist and form C–H bonds on the graphene surface. One can achieve an accurately low-level hydrogenation ($N_{\text{H}} < 0.1\%$ within 0.01% resolution) by optimizing the EB irradiation dose [Fig. 1(a) and (b)].¹⁰ We confirm that the value of N_{H} estimated from the D/G peak height ratios in the Raman spectra is linearly proportional to the EB dose [Fig. 1(b)]. The introduction of this limited disorder leads to the crossover

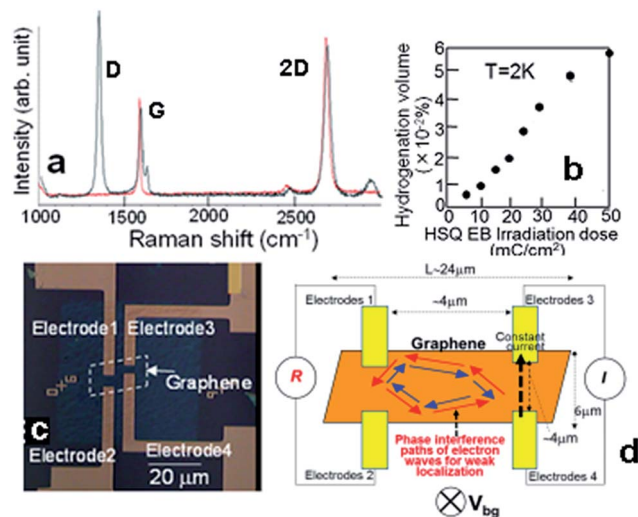


Fig. 1 (a) Example of the Raman spectra of graphene before the HSQ resist treatment (red line) and after EB irradiation (50 mC cm^{-2}) of the HSQ resist (black line). (b) Volume of N_{H} , estimated from the D/G peak height ratios in Raman spectra, as a function of the EB dose incident on an HSQ resist on graphene (ESI.3†). (c) Optical micrograph of the four-probe electrode pattern used for the main measurements. (d) Schematic view of (c) with electron wave trajectories for the WL. Fixed currents of 100 nA have been flowing at the 3–4 electrode pair and R has been measured at the 1–2 electrode pair.

N_{H} regime in which diffusive charge transport appears, while preserving the high quality of the hydrogenated (H)-graphene with a low defect concentration to induce a SOI. An optical micrograph and a schematic view of the four-probe electrode pattern used for the present measurements are shown in Fig. 1(c) and (d), respectively. The resistance (R) has been monitored between the 1–2 electrode pair as a function of the back gate voltage (V_{bg}), when a fixed current flows between the 3–4 electrode pair.

Observation of electrical properties and temperature dependence

The R of H-graphene is shown as a function of V_{bg} and N_{H} in Fig. 2(a). As N_{H} increases, a small, broad R peak appears around $V_{\text{bg}} \sim 13$ V. The peak is dominant in the very low N_{H} region ($< 0.03\%$). Its V_{bg} position roughly agrees with that for the Dirac point (inset) observed at the two-probe measurement at the electrode pair 3–4. In the crossover region ($N_{\text{H}} > 0.03\%$), this peak grows, whereas two other peaks emerge at $V_{\text{bg}} \sim 22$ V and ~ 28 V and grow significantly with increasing N_{H} . These behaviors are very evident in Fig. 2(b). The increase in R peak values is from $\sim 0.06R_{\text{Q}}$ (where $R_{\text{Q}} = h/e^2$ is the resistance quantum) to $0.12R_{\text{Q}}$ for N_{H} values increasing from 0% to $\sim 0.06\%$. A similar correlation has been observed in at least five samples (ESI.2 and 3†).

To clarify the origins of these R peaks, the temperature (T)-dependence of R^{-1} has been measured in the crossover regime ($N_{\text{H}} = 0.06\%$). The semi-logarithmic T -dependence on non-local conductance ($G = R^{-1}$) for the three R peaks shown in Fig. 2(a) is plotted in Fig. 3. The relationship is linear at high T (above ~ 6

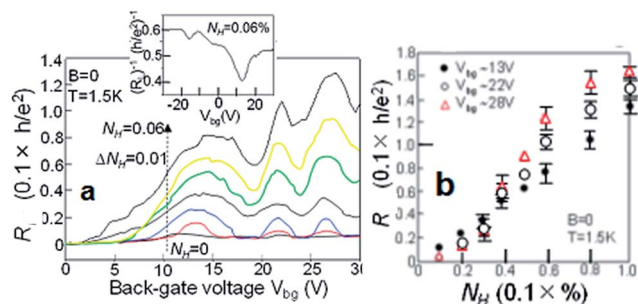


Fig. 2 (a) R of H-graphene as a function of V_{bg} and N_H , observed using the electrode pair 1–2 as shown in Fig. 1(c) and (d). V_{bg} has been swept from 0 V to $+V_{bg}$ to avoid hole-doping through the p-type substrate. Electrons cannot be injected from the surface hydrogen adatoms when $N_H < 0.1\%$. The N_H values of some samples have been tuned by detaching H atoms using high-temperature annealing in a high vacuum. Inset: Dirac point observed in the sample. (b) R vs. N_H for the three R peak values (shown by error bars) observed in (a).

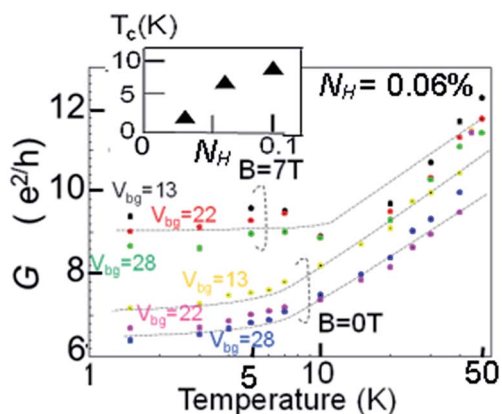


Fig. 3 Semi-logarithmic temperature dependence of the inverse values of the three R peaks shown in Fig. 2(a) for a perpendicular $B = 0$ and 7 T. The sample is in the crossover N_H regime ($N_H = 0.06\%$). The dashed lines are the best fit by the WL formula directly considering the influence of SOI (τ_{SOI}) on T_c (eqn (1)). These WL behaviours are observed only around the three R peaks in Fig. 2(a) (see ESI (7),† which explains the absence of this relationship in the R minima). Inset: T_c between the linear (high T) and saturation (low T) regions of the main panel as a function of N_H .

K), and G saturates below $T \sim 6$ K. This behavior agrees qualitatively with that observed for the WL in CNTs,³ 2DEG, and thin metal films.^{1,2} Quantitatively, the best fit by the conventional WL formula³ gives $p = 4$ for $W = 4 \mu\text{m}$ and $L = 24 \mu\text{m}$ for the present H-graphene (Fig. 1(d)). This p value suggests dephasing of the spin phase interference by electron–electron interactions in the high- T linear dependence region, as in multi-walled CNTs.³ This WL behavior on the T -dependence has not been observed at values of V_{bg} outside of those showing the three R peaks (e.g., around the R minimum; see ESI.4†). This suggests that the phase interference path to create WL (Fig. 1(d)) is formed only at some V_{bg} 's at which carrier densities are controlled *via* the Fermi level shift. V_{bg} satisfies a condition for a constructive phase interference of electron waves.

Significant growth of the R peaks at the higher V_{bg} suggests that larger carrier densities result in the stronger magnitude in the WL.

In Fig. 3, the B_{\perp} also contributes to the dephasing of the interference effects when the Landau orbit size, $L_B = \sqrt{\hbar/eB}$, becomes smaller than $L_{\phi}(T)$. For a sufficiently high B (i.e., when $L_B \ll L_s = \sqrt{D\tau_s}$ (where L_s and τ_s are the spin scattering length and relaxation time, respectively)), the applied B dominates the saturation of conductance at lower T . This is consistent with Fig. 3, which shows a T_c value of ~ 10 K at $B = 7$ T, significantly higher than the value of ~ 6 K measured at $B = 0$ T. The increase in T_c from 6 K to 10 K caused by applying B of 7 T entails a small L_s and a very high τ_s^{-1} in the present graphene. T_c corresponds to the T for which inelastic scattering length (L_{in}) $\approx L_s$ at low B , and to the T for which $L_{in} \approx L_B$ at high B . The B value as high as 7 T gives $L_B \approx L_{in} \sim 0.5 \mu\text{m}$ at $T_c \sim 10$ K. Because L_{in} is proportional to $T^{-p/2}$, L_{in} and, thus, L_s can be estimated as $\sim 2 \mu\text{m}$ at $T = T_c \sim 6$ K for $p = 4$ at $B = 0$ T.

On the other hand, the $T_c \sim 6$ K, which separates the high and low T regions, is significantly different from that of other 2D materials (ESI.5†). $T_c \sim 6$ K observed at $B = 0$ T is considerably higher than the T_c observed in CNTs (e.g., $T_c = 0.3$ K).³ Above the T_c of conventional 2D materials, dephasing is dominated by inelastic scattering factors (electron–electron interaction as mentioned above), while magnetic spin scattering (τ_s^{-1} ; which is T -independent) dominates dephasing below the T_c . Hence, a high T_c (like ~ 6 K) suggests a large τ_s^{-1} rate. However, magnetization measurements by the superconducting quantum interference device have confirmed that our graphene samples mechanically exfoliated from high-quality graphite contain no magnetic impurities. Moreover, T_c increases with increasing N_H (inset of Fig. 3). This cannot be explained simply by the presence of magnetic impurities, which are independent of N_H even if they would be. The origin is discussed later from the viewpoint of the SOI scattering.

Observation of magnetoresistance

When the application of an external B_{\perp} to the graphene plane is applied, observable negative MR directly demonstrates the abovementioned dephasing in the WL. In the presence of a B_{\perp} , negative MRs for the R peak at $V_{bg} \sim 22$ V shown in Fig. 2(a) are observed around $B = 0$ and $T = 1.5$ K in Fig. 4(a) (see ESI.7† for the other two peaks). Because the negative MR denotes a decrease in MR due to dephasing in constructive phase interference with increasing B_{\perp} , it indicates the presence of WL and is consistent with Fig. 3. It should be noted that the negative MR amplitude (i.e., the ratio of MR before and after the drop; $\Delta\text{MR}/\text{MR}$ ($B = 0$)) in the WL decreases with increasing N_H . It is reduced from 10% to $\sim 2.5\%$ when N_H increases from 0% to 0.1% (the black symbols in Fig. 4(b)). This is strange because the slope value of negative MR is conventionally determined only by the WL correction as well as that in conductance at $T > T_c$ in Fig. 3 and should be independent of N_H , when the contribution of SOI is not considered. These negative MRs can only be observed in the three R peaks shown in Fig. 2(a) (ESI. 7†). This is

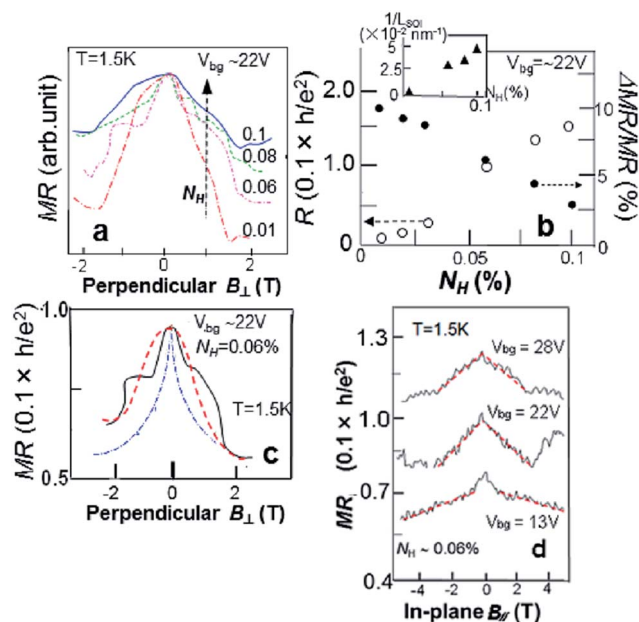


Fig. 4 (a) R vs. B_{\perp} at $V_{bg} \sim 22$ V for samples with different values of N_H , which have been noted for each curve in %. The difference in MR drop ratios is given by $\Delta MR/MR$ ($B = 0$). MR values of individual curves are overlapped at $B = 0$ to directly compare the MR drop ratios. (b) R peak values at $B = 0$ (open symbols for the left axis) and MR-drop amplitude [$\Delta MR/MR$ ($B = 0$)] (black symbols for the right axis) in the WL as a function of N_H . ΔMR is defined as the difference between the values of MR at the peak ($B_{\perp} = 0$) and at the bottom ($B_{\perp} = +2$ T) of individual curves in (b). Inset: L_{SOI} values obtained from the best-fit to the individual curves in (a), using eqn (2)–(4). (c) R vs. B_{\perp} at $V_{bg} \sim 22$ V for the sample with $N_H = 0.06\%$ in Fig. 2(a). The red and blue dotted curves are fits to the data using eqn (2)–(4) using middle-order and weak SOI parameters ($L_{SOI} = 2$ μm and 10 μm , respectively) in the expression for the magnitude of the MR drop. (d) R vs. B_{\parallel} for the three peaks at $N_H = 0.06\%$ of Fig. 2(a). The dotted linear lines are just guides.

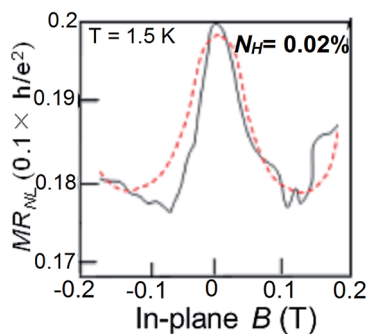


Fig. 5 In-plane B -dependence of the R peak at $V_{bg} = 13$ V for the sample with $N_H = 0.02\%$ in Fig. 2(a). The dotted line is the best fit to the theory of the Larmor spin precession.

consistent with the result of T -dependence in the WL (Fig. 3 and ESI.4†).

Consequently, the high T_c confirmed in Fig. 3 (which increases with increasing N_H) and the negative MR magnitude reduced by increasing N_H in Fig. 4 are unique properties in the present lightly hydrogenated graphene. There are some

possibilities as to reason; *e.g.*, (1) presence of magnetic impurities or defects and (2) presence of possible Rashba-type SOIs. For (1), as mentioned above, ref. 5 reported an enhanced τ_s due to magnetic defects and large-magnitude WL. However, our samples include no magnetic impurities and defects. This has been confirmed using the Raman spectrum and magnetization measurement using SQUID.

On the other hand, for (2), Rashba-type SOIs can be introduced by out-of-plane symmetry-breaking *via* the formation of an sp^3 distortion due to the light hydrogenation of a graphene surface, in spite of the small mass of carbon atoms¹¹ and is discussed here. Some recent theories reported on the correlation of the WL with a SOI. Ref. 9 predicted that effective B of SOI (B_{SOI} ; *i.e.*, a random Rashba field) acts like a magnetic scattering centre. Under a Berry phase factor (β/π) < 0.6 , it predicted that the B_{SOI} results in just suppressed dephasing in the WL without yielding AL (*i.e.*, positive MRs on applied external B_{\perp} and negative G on logarithmic- T dependence) in spite of the presence of SOIs. This is very different from the appearance of AL caused by spin flip and phase shift in π *via* SOIs in conventional 2D materials. Because a value of $\beta/\pi = 0.5$ was previously reported in non H-graphene, the present H-graphene is also expected to actually provide a value of $\beta/\pi < 0.6$ and this theory is applicable. Correlations with electron–phonon interactions also considerably affect the physical properties related to SOIs.^{15–18}

Suppression of dephasing and spin phase protection by SOI

In order to investigate this possibility, we have carried out a data fit using eqn (1) directly incorporating the relaxation time of the SOIs (τ_{SOI}) into T_c and without considering the negative G due to SOI (AL). In ref. 9, a similar correction was taken into consideration for the influence of SOIs to the WL correction when B_{\perp} was applied. The best fit (dashed lines in Fig. 3) gives $T_c'(\tau_{SOI}) = 5.5$ K and $T_c(\tau_s) = 0.5$ K (ESI.5†). This quantitatively supports the strong contribution of the SOIs to the observed high T_c .

$$G(T) = G_0 + \frac{e^2}{2\pi^2\hbar} \frac{W}{L} \ln \left[1 + \left(\frac{T}{T_c(\tau_s) + T_c(\tau_{SOI})} \right)^p \right] \quad (1)$$

This result implies that B_{SOI} at low T suppresses the dephasing arising from electron–electron interactions at high T in the WL. Indeed, T_c increases with increasing N_H as mentioned for the inset of Fig. 3. This is consistent when the B_{SOI} increases with increasing N_H . This also suggests that electron–electron scattering is dominant in the present system, while electron–phonon coupling is weak. This agrees with ref. 13 which reported that SOIs increase the effective mass and decrease G under only weak electron–phonon coupling. Moreover, ref. 14 reported that a B_{SOI} causes spin relaxation, similar to an Elliott–Yafet (EY) mechanism. The value of τ_s^{-1} in this scenario is insensitive to T . This is consistent with the low T region in Fig. 3. In contrast, the D'yakonov–Perel (DY) mechanism becomes insensitive to T , only when electron-impurity scattering is dominant. In the present case, electron-impurity scattering is not dominant because $N_H \ll 0.1\%$. Consequently, the EY-like mechanism should be dominant. This also

agrees with previous reports that the EY mechanism conventionally dominates spin scattering in H-graphene.

Moreover, the dotted red curve in Fig. 4(c) shows an example calculated from the WL-based theory (eqn (2)–(4)),⁴ considering a middle-order of SOI length ($L_{\text{SOI}} \sim 2 \mu\text{m}$ (*i.e.*, when L_s estimated from Fig. 3 is assumed as L_{SOI} ; ESI.6†).

$$\delta G_0 = -\frac{e^2}{\pi h} \frac{W}{L} \left[\left(\frac{1}{2} + \beta \right) (Z_\phi(L_\phi(B))) - \frac{3}{2} Z_\phi(L'_\phi(B)) \right] + \alpha(B) \quad (2)$$

$$Z_\phi(L_\phi(B)) = \ln(L_\phi/l) + 2 \sum k_0 [N(W/L_\phi)] \cos[2\pi N(\Phi/(hc/2e))] \quad (3)$$

$$\frac{1}{L_\phi'^2} = \frac{1}{L_\phi^2} + \frac{2}{L_{\text{SOI}}^2} = \frac{1}{L_\phi^2} + \frac{2}{D\tau_{\text{SOI}}} \quad (4)$$

where β is a constant depending on the electron–electron interaction, L'_ϕ is the phase coherence length considering the L_{SOI} , and $\alpha(B)$ represents the increase or decrease in the mean value of the conductance in eqn (2). The second term of (2) determines a decrease in MR drop ratio with decreasing L_{SOI} (*i.e.*, increasing SOI strength) through eqn (4). In eqn (3), l , k_0 , and Φ are the mean free path, Macdonald function, and magnetic flux ($\pi r^2 H$) penetrating the loop interference path for the WL (Fig. 1(d)) with radius r , respectively. L_ϕ in eqn (3) can be replaced by L'_ϕ .

The dotted red curve actually shows a good agreement with the experimental curve. Although much smaller L_{SOI} (*e.g.*, $\ll 1 \mu\text{m}$) leads to a positive MR and AL in eqn (2)–(4), AL does not appear under this middle-order L_{SOI} in spite of not considering influence of the Berry phase like ref. 9. In contrast, the dotted blue curve obtained using the large $L_{\text{SOI}} \sim 10 \mu\text{m}$ (*i.e.*, weak SOI) exhibits a significantly sharper trend and deviates from the experimental curve. This suggests that the negative MR is also strongly associated with presence of SOI. Indeed, $T = 1.5 \text{ K}$ for this negative MR observation corresponds to the above-mentioned low- T regime ($T < T_c$) in Fig. 3. L_{SOI} values estimated using the data fit to the different N_{H} curves in Fig. 4(a) using the same WL-based theory is shown in the inset of Fig. 4(b). It implies an increase in $1/L_{\text{SOI}}$ with increasing N_{H} and, thus, SOI induced by increasing N_{H} causes the reduction of the negative MR magnitude.

Because the negative MR is caused by dephasing in a constructive phase interference of the WL by increasing external B_\perp , its reduction in the magnitude means suppression of the dephasing due to either protection of the spin moment against the external B_\perp or a possible screening of the external B_\perp by the SOI (or B_{SOI}). As a possible origin, the out-of-plane-symmetric B_{SOI} unique to graphene stabilizes spin moment against an externally applied B_\perp and contributes to the former case. Moreover, when the EY-like mechanism is dominant as mentioned above, it is known that Rashba-type SOI excludes the B_{SOI} from the graphene plane, leading to $\tau_{s\perp} = (1/2)\tau_{s\parallel}$. This also contributes to the suppression of dephasing in the graphene plane.

MRs for the three R peaks shown in Fig. 2(a) (at $N_{\text{H}} = 0.06\%$) are shown as a function of an external in-plane B (B_\parallel) in Fig. 4(d) (ESI.7†). They exhibit a negative and linear dependence. In

contrast to the case of B_\perp [Fig. 4(a)–(c)], B_\parallel basically causes no dephasing and does not change the MRs except for in the case in which a component of B_\parallel is transferred to B_\perp by a strong ripple caused by substrate roughness in the graphene.⁶ Our sample does not correspond to this because it does not lead to the linear slope of the negative MR. Thus, the observed negative MRs are anomalous. The entire linearity is also different from the oscillatory behaviour of the Larmor spin precession, which conventionally appears with presence of SOI under applied B_\parallel .

This negative MR with the linear slope can be qualitatively understood using a theory that out-of-plane-symmetric SOIs unique to graphene are linearly reduced by coupling with the in-plane Zeeman effect, which increases with increasing B_\parallel .¹⁶ In our samples, the dephasing in a constructive phase interference of the WL is suppressed by the SOIs at $B = 0$ and $T = 1.5 \text{ K}$ (*i.e.*, $T < T_c$), as explained for Fig. 3, resulting in MR values (at $B = 0$) larger than those without the suppression of dephasing. With increasing B_\parallel , SOIs linearly decrease by coupling with the in-plane Zeeman effect. Then, the dephasing suppressed by SOI is also linearly reduced and, thus, the dephasing recovers, resulting in the linear decrease in MR.¹⁶

Finally, possible evidence for the presence of the SOI is shown in Fig. 5. The in-plane B -dependence of the small R peak around $V_{\text{bg}} = 13 \text{ V}$ in Fig. 2(a) is shown for $N_{\text{H}} = 0.02\%$ sample in Fig. 5. The plot exhibits oscillatory behavior. This behavior agrees with the Larmor spin-precession theory, as shown by the dotted calculation curve ($\omega_{\text{B}} = \Gamma \Delta B \leq D_s/W^2$, where Γ is the gyromagnetic ratio, ΔB is the oscillation period, W is the width of the sample, and D_s is the spin diffusion coefficient). This agreement provides possible evidence for the presence of SOIs in this low N_{H} sample ($< 0.3\%$) within a ballistic charge transport regime. Our diffusive samples have low values of electron mobility μ ($< \sim 10\,000 \text{ cm}^2 \text{ V}^{-1} \text{ s}^{-1}$), resulting in a small value of D_s/W^2 ($W = 4 \mu\text{m}$) because $\mu \propto D_s$. However, the small value of ΔB ($\sim 0.2 \text{ T}$) satisfies the condition $\omega_{\text{B}} = \Gamma \Delta B \leq D_s/W^2$ if we use the previously measured values of Γ . This SOI should survive even in larger N_{H} samples ($> 0.4\%$), which are within a crossover regime between ballistic and diffusive regimes. However, this measurement has been performed in the four-probe pattern shown in Fig. 1. Because it cannot exclude the possible influence of the diffusion current entirely, a very accurate measurement is indispensable.

Conclusions

In summary, we have lightly hydrogenated graphene ($0\% < N_{\text{H}} \ll 0.1\%$) by precisely controlling the dose of EB irradiation to a HSQ resist treated on graphene and revealed the presence of the linear relationship for N_{H} vs. EB dose. The three R peaks have been observed depending on V_{bg} with increasing N_{H} . Semi-logarithmic- T and B_\perp dependence of the peaks in samples with $N_{\text{H}} = 0.06\%$ have indicated the presence of WL, while the T_c (separating the high and low T regions (*i.e.*, electron–electron interaction and spin scattering T regimes, respectively)) as high as 6 K and the negative MR magnitude reduced by increasing N_{H} were confirmed as distinctive properties of the WL, which suggest the suppression of dephasing (*i.e.*, protection of spin

phase) in the WL. As an origin, correlation of the WL with Rashba-type SOI has been discussed. If the random Rashba-type SOI, introduced by the out-of-plane symmetry breaking due to the creation of sp^3 bonds driven from the small N_{H} , would act like a magnetic scattering centre, it leads to enhancement of the τ_{SOI} ($L_{\text{SOI}} \sim 2 \mu\text{m}$) and the suppression of dephasing in the WL against the electron–electron interaction-based dephasing on T -dependence and the magnetic dephasing caused by externally applied B_{\perp} , because the SOI in graphene has a complete out-of-plane symmetry and excludes the B_{SOI} from the graphene plane under the EY-like mechanism. This is qualitatively consistent with a previous work,¹² which reported that the plasma-hydrogenated graphene with $N_{\text{H}} = 0.02\%$ exhibited a significant increase in the L_s as large as $\sim 7 \mu\text{m}$ due to the Rashba-type SOIs. Although much careful investigation is indispensable to confirm the presence of the SOI (*e.g.*, observation of Hanle effect and Larmor spin precession entirely excluding influence of diffusion current), the present findings in lightly hydrogenated graphene must be valuable for graphene spintronics, which requests a long spin diffusion- and coherence-length on the SiO_2 substrate.^{7,8} It will also lead to the realization of a 2D-topological insulating state in graphene.^{17–19}

Acknowledgements

The authors thank S. Murakami, Y. Otani, T. Enoki, Y. Shimazaki, M. Yamamoto, S. Tarucha, H. Shinohara, T. Ando, H. Hibino, P. Herrero, P. Seneor, A. H. Macdonald, R. Wiesendanger, S. Roche, and M. S. Dresselhaus for their technical contribution, fruitful discussions, and continuous encouragement. The work at Aoyama Gakuin was partly supported by a Grant-in-aid for Scientific Research (15K13277, 24241046) in MEXT and AOARD grant (135049) in U.S. Air Force Office of Scientific Research. The work in the University of Tokyo was

also supported by Grant-in-Aid for Scientific Research on Innovative Area, “Nano Spin Conversion Science” (Grant No. 26103003), and by Grants No. 25247051 and No. 15K17676.

Notes and references

- 1 T. Ando, *et al.*, *Mesoscopic physics and electronics. Nano Science and Technology series*, ed. v. K. Klitzing and R. Wiesendanger, Springer-Verlag, 1998.
- 2 Y. Imry, *Introduction to mesoscopic physics*, Oxford University Press, Oxford, 2002.
- 3 L. Langer, V. Bayot, E. Grivei and J.-P. Issi, *Phys. Rev. Lett.*, 1996, **76**, 479.
- 4 J. Haruyama, I. Takesue and T. Hasegawa, *Phys. Rev.*, 2001, **65**, 033402.
- 5 M. B. Lundeberg, *et al.*, *Phys. Rev. Lett.*, 2013, **110**, 156601.
- 6 M. B. Lundeberg, *et al.*, *Phys. Rev. Lett.*, 2010, **105**, 146804.
- 7 A. V. Kamalakar, *et al.*, *Nat. Commun.*, 2015, **6**, 6766.
- 8 B. Dlubak, P. Seneor, A. Fert, *et al.*, *Nat. Phys.*, 2012, **8**, 557.
- 9 W.-Y. Shan, *et al.*, *Phys. Rev.*, 2012, **86**, 125303.
- 10 T. Kato, T. Nakamura, J. Haruyama, *et al.*, *Appl. Phys. Lett.*, 2014, **104**, 252410.
- 11 J. Balakrishnan, *et al.*, *Nat. Phys.*, 2013, **9**, 284–287.
- 12 M. Wojtaszek, *et al.*, *Phys. Rev.*, 2013, **87**, 081402(R).
- 13 Z. Li, L. Covaci, M. Berciu, D. Baillie and F. Marsiglio, *Phys. Rev.*, 2011, **83**, 195104.
- 14 P. Zhang and M. W. Wu, *New J. Phys.*, 2012, **14**, 033015.
- 15 Z. Li and J. P. Carbotte, *Phys. Rev.*, 2013, **88**, 045417.
- 16 E. McCann and V. I. Fal’ko, *Phys. Rev. Lett.*, 2012, **108**, 166606.
- 17 J. Sinova, *et al.*, *Phys. Rev. Lett.*, 2004, **92**, 126603.
- 18 S. Murakami, N. Nagaosa and S. C. Zhang, *Science*, 2003, **301**, 1348.
- 19 C. L. Kane and E. J. Mele, *Phys. Rev. Lett.*, 2005, **95**, 226801.